Cerebral Cortex, September 2017;27: 4303–4313

doi: 10.1093/cercor/bhw230
Advance Access Publication Date: 6 August 2016
Original Article

ORIGINAL ARTICLE

The Cytokine CXCL12 Promotes Basket Interneuron Inhibitory Synapses in the Medial Prefrontal Cortex

Pei-Rung Wu[1], Kathleen K.A. Cho[1,2,3], Daniel Vogt[1], Vikaas S. Sohal[1,2,3], and John L.R. Rubenstein[1]

[1]Department of Psychiatry, University of California, San Francisco, San Francisco, CA 94143, USA, [2]Center for Integrative Neuroscience, University of California, San Francisco, San Francisco, CA 94143, USA, and [3]Sloan-Swartz Center for Theoretical Neurobiology, University of California, San Francisco, San Francisco, CA 94143, USA

Address correspondence to Pei-Rung Wu and John L.R. Rubenstein, Department of Psychiatry, University of California, San Francisco, 1550 4th Street, Room 284C, Box 2611, San Francisco, CA 94158-2324, USA. Email: f93448001@ntu.edu.tw, pei-rung.wu@ucsf.edu/john.rubenstein@ucsf.edu

Abstract

Prenatally, the cytokine CXCL12 regulates cortical interneuron migration, whereas its postnatal functions are poorly understood. Here, we report that CXCL12 is expressed postnatally in layer V pyramidal neurons and localizes on their cell bodies in the medial prefrontal cortex (mPFC), while its receptors CXCR4/CXCR7 localize to the axon terminals of parvalbumin (PV) interneurons. Conditionally eliminating CXCL12 in neonatal layer V pyramidal neurons led to decreased axon targeting and reduced inhibitory perisomatic synapses from PV^+ basket interneurons onto layer V pyramidal neurons. Consequently, the mPFC of *Cxcl12* conditional mutants displayed attenuated inhibitory postsynaptic currents onto layer V pyramidal neurons. Thus, postnatal CXCL12 signaling promotes a specific interneuron circuit that inhibits mPFC activity.

Key words: axon targeting, CXCR4/CXCR7, layer V pyramidal neurons, parvalbumin interneurons, schizophrenia

Introduction

The proper balance of excitation and inhibition in the prefrontal cortex (PFC) is essential for optimal cognitive functioning (Uhlhaas and Singer 2010; Cho and Sohal 2014). Disturbances in PFC inhibitory gamma-aminobutyric acid-containing (GABAergic) cortical interneurons (CINs), such as those expressing parvalbumin (PV) and somatostatin (SST), are implicated in neuropsychiatric disorders, including schizophrenia (Lewis et al. 2012; Volk and Lewis 2014). PV^+ and SST^+ CINs are generated in the medial ganglionic eminence (MGE), from where they tangentially migrate in the prenatal mouse brain [embryonic day (E) ~12–18]. Once in the cortex, they radially migrate into their appropriate layers [~E18–postnatal day (P) 6], where they receive and make synaptic connections with excitatory pyramidal neurons (Bartolini et al. 2013).

The axons from diverse CIN subtypes form synapses with different subdomains of pyramidal neurons. For example, layer V pyramidal neuron somata are innervated by PV^+ basket CINs, while PV^+ chandelier CINs target the axon initial segments (AIS), and SST^+ Martinotti CINs innervate distal dendrites (Huang et al. 2007). These processes are controlled by transcription factors (Kessaris et al. 2014), and extracellular cues such as cytokine and neuregulin signaling (Marin 2013).

The cytokine C-X-C motif ligand 12 (CXCL12; also known as stromal cell-derived factor-1, SDF-1) regulates the immune system (Nagasawa et al. 1996; Ara et al. 2003; Greenbaum et al. 2013), and the nervous system (Marin 2013). In embryonic mouse neocortex, *Cxcl12* is expressed in the meninges and the subventricular zone/intermediate zone (SVZ/IZ), where it attracts CINs and directs their tangential migration along two

pathways (Stumm et al. 2003; Tiveron et al. 2006; Sanchez-Alcaniz et al. 2011; Wang et al. 2011; Abe et al. 2015). In vitro studies suggest that CXCL12 enhances neurite outgrowth and axon pathfinding of entorhinal pyramidal neurons to the dentate gyrus, and regulates the formation of excitatory synapses in the dentate gyrus (Ohshima et al. 2008). In addition, in vivo studies show that CXCL12 promotes thalamocortical axon growth prenatally (Abe et al. 2015). In the adult dentate gyrus, CXCL12 is proposed to function as a neurotransmitter where it potentiates GABAergic signals (Bhattacharyya et al. 2008). While CXCL12 functions in prenatal brains and adult dentate gyrus have been investigated, its function(s) during postnatal neocortical development are unknown.

CXCL12 has two known receptors expressed by developing CINs: CXC receptor 4 (CXCR4) and CXC receptor 7 (CXCR7). They control CIN tangential migration to and within the cortex (Li et al. 2008; Sanchez-Alcaniz et al. 2011; Wang et al. 2011; Sanchez-Martin et al. 2013), and have been postulated to regulate CIN radial migration and laminar positioning (Vogt et al. 2014). *Cxcr4* and *Cxcr7* continue to be expressed postnatally in mouse neocortex (Tiveron et al. 2010). Importantly, abnormal *Cxcr4*/*Cxcr7* expression has been reported in the postmortem PFC from schizophrenia subjects (Volk et al. 2015). Furthermore, *Cxcl12* expression has been detected in the postnatal neocortex (Tiveron et al. 2010; Vogt et al. 2014), where its function has not yet been determined.

Here, we report that CXCL12 protein surrounds the somata of layer V pyramidal neurons in the postnatal mouse medial PFC (mPFC), while its receptors, CXCR4/CXCR7, are expressed in the axon terminals of CINs. Conditional elimination of CXCL12 in layer V pyramidal neurons during early postnatal ages reduced PV^+ basket interneuron axon targeting to the pyramidal somata, and decreased the number of inhibitory perisomatic synaptic punctae and inhibitory postsynaptic currents (IPSCs) onto layer V pyramidal neurons. Thus, postnatal CXCL12 signaling promotes PV^+ basket CIN synapses and inhibition onto mPFC layer V pyramidal neurons. Notably, this study identifies a novel role for CXCL12 signaling in regulating mPFC activity and suggests a molecular mechanism for neuropsychiatric disorders.

Materials and Methods

Mice

All animal care and procedures were performed according to the University of California at San Francisco (UCSF) Laboratory Animal Research Center guidelines. Mice were housed at a density of 2–5 adults/cage or 1–2 adults with 1 litter/cage. The light–dark cycle was 12:12 hours. All mice strains have been previously reported: *Cxcl12*$^{GFP/+}$ (Ara et al. 2003), *Nkx2.1-Cre* (Xu et al. 2008), *Ai14* (Madisen et al. 2010), and *Cxcl12*$^{flox/+}$ (Greenbaum et al. 2013). *Rbp4-Cre* was obtained from the Gene Expression Nervous System Atlas Project (GENSAT, founder line KL100). *Cxcl12*$^{GFP/+}$ and *Nkx2.1-Cre* mice were maintained on a CD-1 background, while the other strains were on a C57BL/6J background. Mice of both genders were used.

Histology

Embryos were removed from pregnant females. Next, the embryonic brains were dissected and fixed in 4% paraformaldehyde (PFA) in phosphate-buffered saline (PBS) at 4 °C overnight. For postnatal study, animals were anaesthetized with CO_2 (>P3) or ice (<P3), and perfused with PBS, followed by 4% PFA in PBS. The brains were then removed and post-fixed in the same fixative for 3 h. Fixed brains were sectioned at a thickness of 50 μm with a vibratome (Leica VT1200S; Leica).

For immunohistochemistry (IHC), free-floating sections were washed with PBS supplemented with 3% H_2O_2, 10% methanol, and 0.25% Triton X-100 for 15 min to quench endogenous peroxidases. Sections were then incubated with a blocking solution (5% normal goat serum or horse serum, 0.25% Triton X-100, and 0.2% gelatin in PBS) for 2 h, primary antibodies at 4°C overnight, and secondary antibodies for 2 h. Sections were incubated in ABC solution (Vector Laboratories) for 1 h, rinsed three times in PBS, and placed into 0.005% 3,3′-diaminobenzidine tetrahydrochloride (DAB; Sigma) with 0.001% H_2O_2 in PBS for 3–5 min. Reactions were stopped with PBS. Sections were washed, mounted, air-dried overnight, and coverslipped with Permount (Fisher Scientific).

For immunofluorescence, sections were blocked with 5% BSA and 0.25% Triton X-100 in PBS for 2 h, incubated with the primary antibodies at 4°C overnight, and then with secondary antibodies for 2 h. Sections were washed, mounted, and coverslipped with mounting medium with DAPI (Vector Laboratories). All primary and secondary antibodies were diluted in blocking solutions.

Antibodies

Primary antibodies: chicken anti-GFP (1:2000, Aves Lab, #GFP-1020); goat anti-somatostatin (1:400, Santa Cruz, #sc-7819), goat anti-CXCL12 (1:200, Santa Cruz, #sc-6193) (Bhattacharyya et al. 2008); mouse anti-GAD65 (1:500, Millipore, #MAB351) (Fazzari et al. 2010), mouse anti-CXCR7 (11G8, 1:200, R&D Systems, #MAB42273) (Sanchez-Alcaniz et al. 2011); rabbit anti-GFP (1:2000, Invitrogen, #A11122), rabbit anti-parvalbumin (1:2000, Swant, #PV 25) (Vogt et al. 2014), rabbit anti-phospho-IκBα (14D4, 1:300, Cell Signaling, #2859) (Fazzari et al. 2010); rat anti-RFP (5F8, 1:2000, ChromoTek, #5f8), rat anti-CXCR4 (1:200, BD biosciences, #551852). The IHC secondary antibodies were biotinylated goat anti-rabbit or horse anti-goat (1:200, Vector Laboratories), and the immunofluorescence secondary antibodies were Alexa Fluor 488-, 594-, or 647-conjugated (1:300, Invitrogen).

Image Acquisition and Quantification

IHC images were captured by a Coolsnap camera (Photometrics) mounted on a microscope (Eclipse 80i; Nikon) with a ×10 objective, using NIS Elements acquisition software (Nikon). Immunofluorescence Images were taken by a confocal laser-scanning microscope (LSM 700; Zeiss) with a ×10, ×20, or ×63 objective lens or by a Zeiss Axio Imager.M1m with a ×5 objective, using the ZEN 2010 software (Zeiss). Orthogonal dimension images of perisomatic PV^+ or $GAD65^+$ punctae were generated with the software ZEN 2009 Light Edition (Zeiss). ImageJ software (NIH) was used to measure the length of AIS and distal dendrites of pyramidal neurons. Density of punctae represents the number of punctae per length of each AIS or distal dendrite.

MGE Transplantation

MGE transplantations were done as previously described (Vogt et al. 2015). Briefly, E14.5 MGEs were mechanically dissociated, pelleted, and transplanted into P2 *Cxcl12 CKO* and control neocortex. Each host received six injections of 70 nl per site.

Slice Preparation

Slice preparation and intracellular recording followed our published protocol (Sohal and Huguenard 2005). Coronal slices, 250 μm thick, from P42–49 mice of either sex were cut in a chilled slicing solution in which Na^+ was replaced by sucrose, then incubated in warmed ACSF at 30–31°C for 15 min and then at least 1 h at room temperature before being used for recordings. ACSF contained (in mM): 126 NaCl, 26 $NaHCO_3$, 2.5 KCl, 1.25 NaH_2PO_4, 1 $MgCl_2$, 2 $CaCl_2$, and 10 glucose. Slices were secured by placing a harp along the midline between the two hemispheres.

Intracellular Recording

Somatic whole-cell patch recordings were obtained from visually identified neurons in layer V of infralimbic or prelimbic cortex using differential contrast video microscopy on an upright microscope (BX51WI; Olympus). Recordings were made using a Multiclamp 700A (Molecular Devices). Patch electrodes (tip resistance = 2–6 MOhms) were filled with the following (in mM): 130 K-gluconate, 10 KCl, 10 HEPES, 10 EGTA, 2 $MgCl_2$, 2 MgATP, and 0.3 NaGTP (pH adjusted to 7.3 with KOH). All recordings were at 32.5 ± 1 °C. Series resistance was usually 10–20 MΩ, and experiments were discontinued above 30 MΩ. Experiments were performed blind to genotype.

Injection of Virus for DlxI12b-mCherry Expression

To visually identify interneurons, we injected an adeno-associated virus (AAV) vector that drives mCherry expression using the *DlxI12b* enhancer, which restricts expression to GABAergic interneurons (Potter et al. 2009; Lee et al. 2014) (hereafter abbreviated as *I12b*). We injected 0.5 μl of virus following previously-described procedures (Sohal et al. 2009). We waited at least 4 weeks after virus injection before preparing brain slices. Coordinates for injection into mPFC were (in millimeters relative to bregma): 1.7 anterior-posterior, 0.3 mediolateral, and −2.75 dorsoventral. Injections were performed blind to genotype.

Injection of Virus for ChR2 Expression

To express ChR2 specifically in interneurons, we used an AAV that drives *I12b*-dependent expression of a ChR2-eYFP fusion protein (Cho et al. 2015). For the in vitro slice experiments, we injected 0.75 μl of virus following previously-described procedures (Sohal et al. 2009), then waited at least 4 weeks after virus injection before preparing brain slices. For experiments in which we recorded from ChR2-negative pyramidal neurons while stimulating ChR2 in interneurons (labeled using *I12b*), we injected virus into the mPFC and verified that we observed fluorescent somata on the injected side (which was the location for recording). Coordinates for injection into mPFC were (in millimeters relative to bregma): 1.7 anterior-posterior, 0.3 mediolateral, and −2.75 dorsoventral. Injections were performed blind to genotype.

In Vitro ChR2 Stimulation

We stimulated ChR2 in interneurons using ~4–5 mW flashes of light generated by a Lambda DG-4 high-speed optical switch with a 300 W Xenon lamp (Sutter Instruments), and an excitation filter set centered around 470 nm, delivered to the slice through a ×40 objective (Olympus). Illumination was delivered across a full high-power (×40) field. To measure inhibitory currents, we made voltage-clamp recordings at a holding potential of +10 mV while stimulating ChR2 using trains of light flashes (5 ms/flash, 40 Hz). Experiments were performed blind to genotype.

Analysis of Intrinsic Properties

Intrinsic properties were calculated based on the current clamp responses to a series of 250 ms current pulse injections from −200 to 450 pA (50 pA/increment). Input resistance was calculated from the voltage response to a −50 pA, 250 ms current pulse. Spiking properties were calculated based on the response to a current pulse that was 100 pA above the minimal level that elicited spiking.

As described above, we identified interneurons based on the expression of mCherry driven by AAV and the *DlxI12b* enhancer (Potter et al. 2009). Recorded interneurons were therefore subdivided into fast-spiking (FS) or non-FS based on electrophysiological properties. Specifically, we classified an interneuron as FS if the adaptation ratio was <1.3, and the input resistance was <350 MOhms. Type A neurons were distinguished by their voltage sag and rebound afterdepolarization (ADP) following hyperpolarizing current pulses (−200 pA, 250 ms): type A neurons were defined based on a combined sag and rebound ADP >2.5 mV.

Statistics

Data were analyzed using Prism 6 (Graph Pad), SPSS 15 (IBM), and Excel (Microsoft). Lamination data were analyzed using two-tailed χ^2 test, while the other data, which followed a normal distribution, were analyzed using two-tailed unpaired Student's *t*-test with or without Welch's correction, depending on the results of variance tests (*F*-test). $P < 0.05$ was considered statistically significant.

Results

Cxcl12 is Expressed Postnatally in Layer V Pyramidal Neurons

Neocortical *Cxcl12* expression was assessed in postnatal mice (P1-P84) using the $Cxcl12^{GFP}$ allele, in which *GFP* was expressed under the control of the endogenous *Cxcl12* locus (*GFP* knockin mice; Ara et al. 2003). CXCL12-GFP was expressed in the meninges, blood vessel endothelial cells, and layer V pyramidal neurons (Ara et al. 2003; Vogt et al. 2014) (Fig. 1*a*–*f* and Supplementary Fig. 2a–b), but not in PV^+ or SST^+ CINs (Supplementary Fig. 2c–c" and d–d"). While meningeal CXCL12-GFP gradually decreased after P7, CXCL12-GFP persisted in layer V pyramidal neurons (Vogt et al. 2014) (Fig. 1*c*–*f*). During this postnatal period, CINs migrate radially to specific cortical layers. We explored whether CXCL12 expression by layer V pyramidal neurons regulated CIN radial migration. $Cxcl12^{flox/+}$ mice, which carry the *Cxcl12* conditional allele (Greenbaum et al. 2013), were crossed to *Rbp4-Cre* mice. Within the neocortex, *Rbp4-Cre* is specifically expressed in layer V pyramidal neurons (GENSAT). *Rbp4-Cre* activity was detected using the *Ai14* reporter ($Ai14^{flox/+}$), which expresses tdTomato following Cre-mediated recombination (Madisen et al. 2010). *Rbp4-Cre* neocortical activity was first detected at E17.5 (Fig. 1*a'*–*a'''* and Supplementary Fig. 1b). In the somatosensory cortex, ~56% of CXCL12-GFP^+ neurons co-expressed tdTomato at P1, and this increased to ~75% after P7, suggesting that ~75% of CXCL12-GFP^+

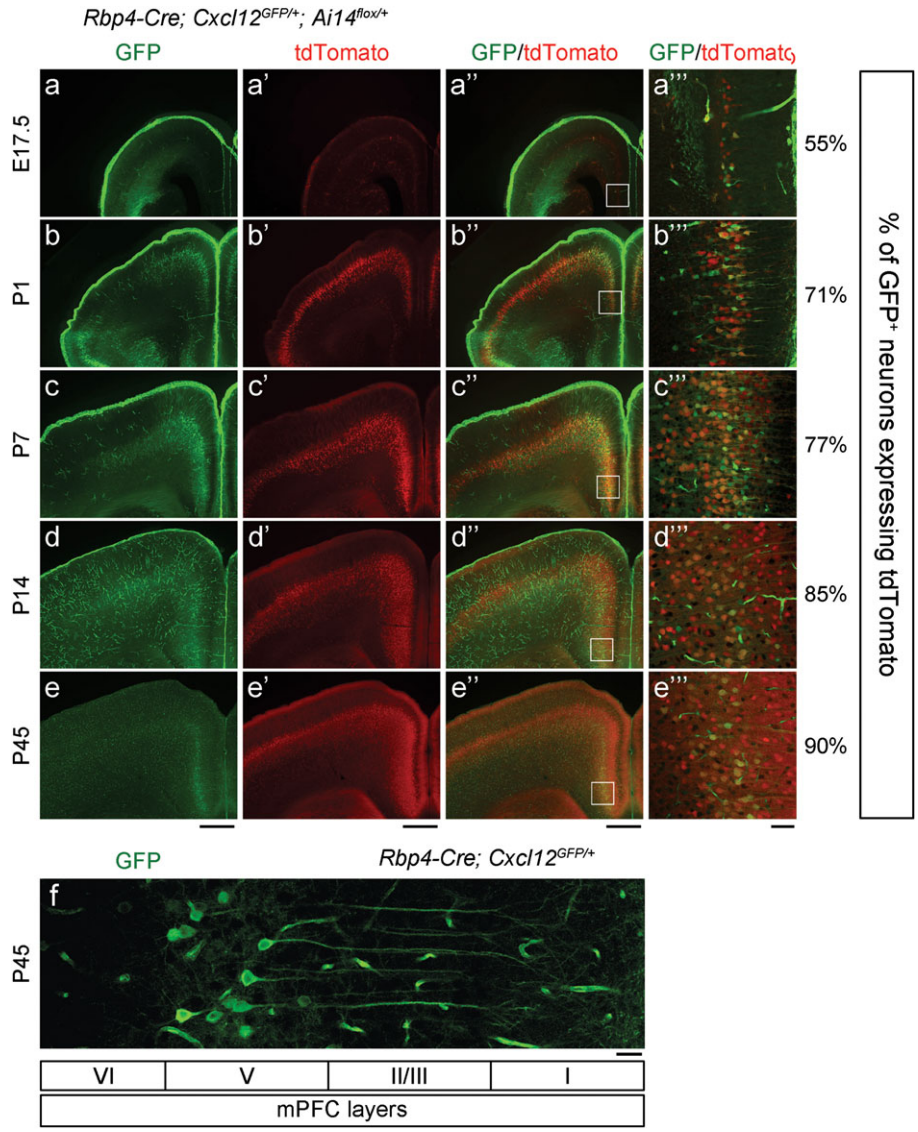

Figure 1. *Cxcl12* is expressed in layer V pyramidal neurons. (*a–e, a'–e'*, and *a"–e"*) Epifluorescent images in coronal sections show the expression pattern of CXCL12-GFP and Rbp4-Cre in the cortex. GFP labeled the cells which expressed *Cxcl12*, whereas tdTomato (red) labeled Cre$^+$ cells. Scale bars, 500 μm. (*a"'–e"'*) Confocal images of the regions within the white rectangles in (a"–e") indicate the expression of CXCL12-GFP and Rbp4-Cre in mPFC layer V pyramidal neurons. Quantification shows the percentage of CXCL12-GFP$^+$ pyramidal neurons which co-expressed tdTomato. Scale bar, 50 μm. (*f*) Single confocal image shows CXCL12-GFP labeled layer V pyramidal neurons and blood vessel endothelial cells in the P45 mPFC. Layer IV is thought not be present in the mPFC. Scale bar, 25 μm. See also Supplementary Fig. 1a for schematic of the regions imaged.

layer V pyramidal neurons co-expressed Rbp4-Cre at P7 (Supplementary Fig. 1a–b).

Next, we examined CIN lamination using immunohistochemistry for SST at P7 and P14, and PV at P14. We found no differences in the lamination pattern of SST$^+$ and PV$^+$ CINs in the somatosensory cortex between *Rbp4-Cre; Cxcl12*$^{GFP/+}$ (control) and *Rbp4-Cre; Cxcl12*$^{GFP/flox}$ (*Cxcl12* conditional knockout, termed *Cxcl12 CKO* hereafter) (Supplementary Fig. 1c–e). On the contrary, when we challenged *Cxcl12 CKO* by transplanting E14.5 MGE (source of PV$^+$ and SST$^+$ CINs) labeled using *Nkx2.1-Cre; Ai14*$^{flox/+}$ into P2 control and *Cxcl12 CKO* neocortex, we observed that *Cxcl12 CKO* had an increased fraction of the transplanted cells in layer II/III and a decreased fraction in layer V at 7 days post-transplantation (DPT7). Thus, CXCL12 can regulate neocortical lamination of *Nkx2.1*-lineage CINs derived from transplanted MGE cells (Supplementary Fig. 1f–g).

CXCL12 Localizes on the Extracellular Surface of Pyramidal Neuron Cell Bodies, while CXCR4/7 are Present on CIN Axon Terminals in the mPFC

Next, we explored whether CXCL12 expression by layer V pyramidal neurons regulated other CIN properties. We focused on the mPFC, rather than other cortical areas, because after P14, CXCL12-GFP was greatly reduced in cortical areas other than the mPFC until P84 (Fig. 1*a–e* and Supplementary Fig. 2a–b). In the P14 mPFC, ~85% of CXCL12-GFP$^+$ neurons co-expressed tdTomato (Fig. 1*d–d"'*), providing evidence that most CXCL12-GFP$^+$ layer V pyramidal neurons co-expressed Rbp4-Cre.

The elimination of CXCL12 in *Cxcl12 CKOs* was confirmed using immunofluorescence. In the P45 *Cxcl12 CKO* mPFC, ~84% of CXCL12-GFP$^+$ pyramidal neurons had reduced CXCL12 (Fig. 2a, a', b, and b'), consistent with the fact that ~85% of CXCL12-GFP$^+$ layer V pyramidal neurons co-expressed Rbp4-Cre

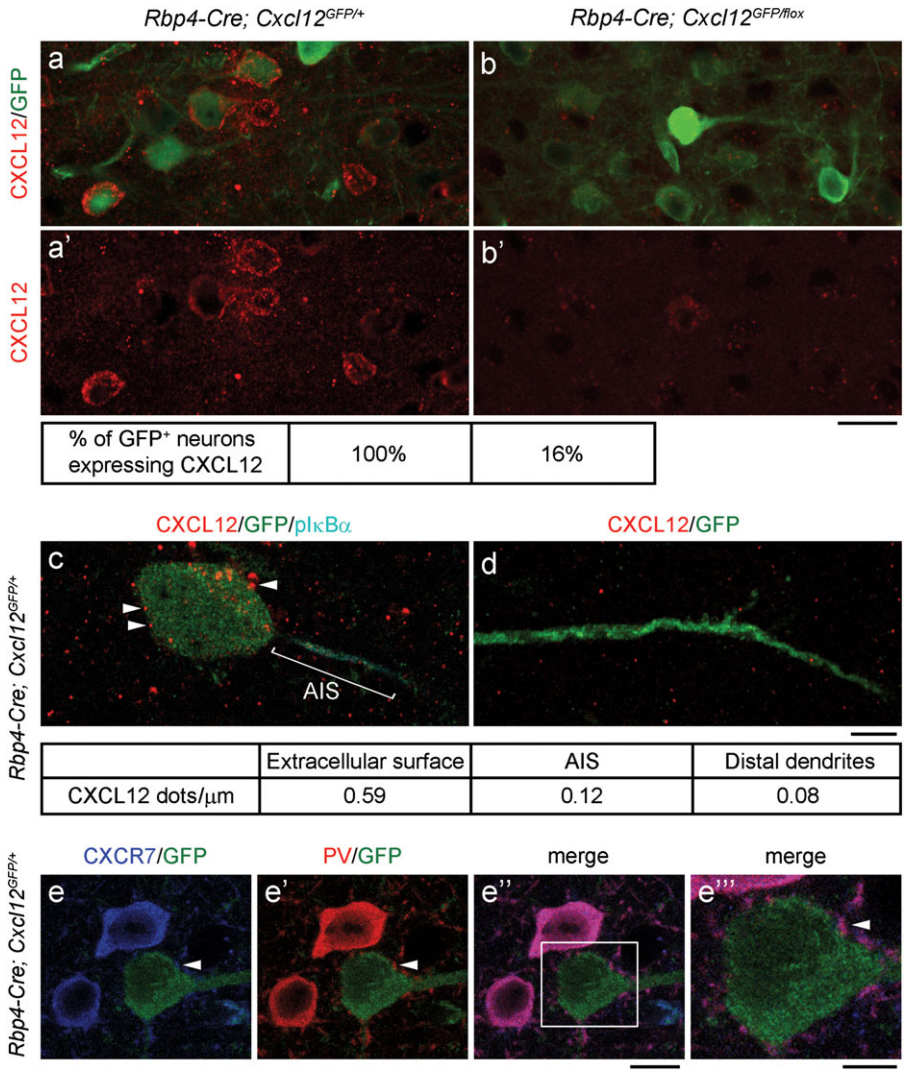

Figure 2. CXCL12 localizes on the extracellular surface of pyramidal neuron cell bodies, while CXCR7 is present at PV$^+$ interneuron axon terminals in the P45 mPFC. (*a*, *a'*, *b*, and *b'*) Confocal images show CXCL12 (red) reduction in *CXCL12 CKO* layer V pyramidal neurons (labeled by GFP). Scale bar, 20 μm. (*c*–*d*) Confocal images show that CXCL12 dots (red, indicated by arrowheads) mainly localized on the extracellular surface and inside the cell body (c), while fewer CXCL12 dots were found on the AIS (c, labeled by pIκBα, cyan) and distal dendrites (d, labeled by GFP) of layer V pyramidal neurons. Density of CXCL12 dots represents the number of CXCL12 dots per length of cell body circumference or AIS or distal dendrites. Scale bar, 5 μm. (*e*–*e''*) Confocal images show that CXCR7 (blue) localized in the cell bodies and axon terminals of PV$^+$ (red) interneurons. GFP labeled layer V pyramidal neurons encircled by PV$^+$ axon terminals (indicated by arrowheads). Scale bar, 10 μm. (*e'''*) The high-magnification image of the region within the white rectangle in (e''). Scale bar, 5 μm.

(Fig. 1*d'''*–*e'''*). Next, we investigated subcellular CXCL12 and CXCR4/7 expression in the postnatal mPFC. We found that most CXCL12 appeared around the extracellular surface or inside the cell bodies of layer V pyramidal neurons, while less CXCL12 was detected on the AIS [labeled by phospho-IκBα (pIκBα)] (Fazzari et al. 2010) and distal dendrites in layer I (Fig. 2*c*–*d*). Both CXCR4 and CXCR7 were found in the cell bodies and all of the assessed axon terminals of PV$^+$ interneurons (Fig. 2*e*–*e'''* and Supplementary Fig. 3a–a''').

CXCL12 Promotes Targeting of PV$^+$ CIN Axons to Layer V Pyramidal Neurons in the mPFC

We next studied targeting of PV$^+$ interneuron axons using PV immunofluorescence and confocal imaging. PV$^+$ axon terminal punctae encircled the cell bodies of CXCL12-GFP$^+$ pyramidal neurons in control mPFCs (Fig. 3*a*, right panel). The number of perisomatic PV$^+$ punctae was decreased ~28% in *Cxcl12 CKOs* (Fig. 3*a*–*b* and Supplementary Fig. 4a–c), providing evidence that CXCL12 promotes targeting of PV$^+$ CIN axons to layer V pyramidal neurons in the mPFC.

CXCL12 Enhances Inhibitory Perisomatic Synapses onto mPFC Layer V Pyramidal Neurons

To determine whether the decreased axon targeting led to a reduction of inhibitory synapses onto layer V pyramidal neurons, we used immunofluorescence with the inhibitory presynaptic marker, glutamate decarboxylase 65 (GAD65) (Fazzari et al. 2010). Confocal z-stack images showed that *Cxcl12 CKO* had a ~31% reduction in the number of perisomatic GAD65$^+$ punctae at P16 (Supplementary Fig. 5a–b). These results indicate that CXCL12 promotes the formation of inhibitory perisomatic synapses onto layer V pyramidal neurons. Furthermore,

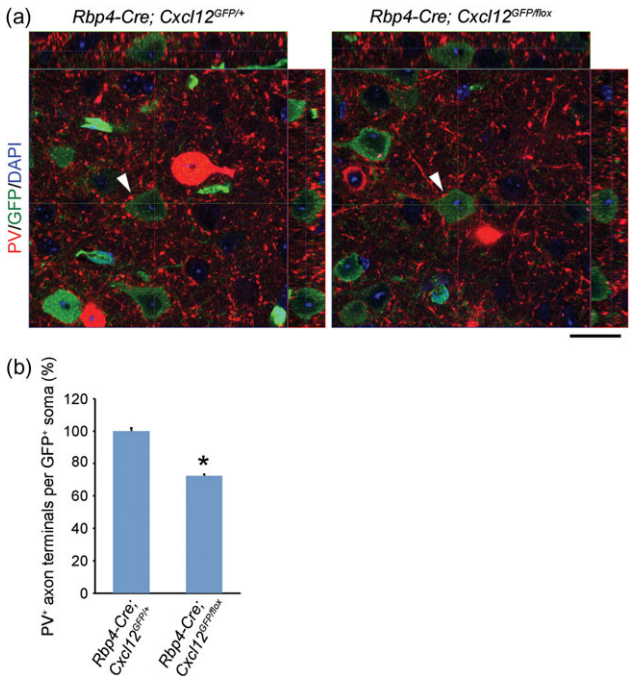

Figure 3. CXCL12 promotes targeting of PV$^+$ interneuron axons to layer V pyramidal neurons in the P45 mPFC. (*a*) Orthogonal projections from confocal z-stack images (0.5 μm intervals) show a reduction of perisomatic PV$^+$ axon terminals onto CXCL12-GFP$^+$ pyramidal neurons in *Cxcl12 CKOs*. PV (red) labeled both cell bodies and axon terminals of PV$^+$ interneurons. Arrowheads indicate pyramidal neurons examined. Scale bar, 20 μm. (*b*) Quantification of PV$^+$ axon terminals on the cell bodies of CXCL12-GFP$^+$ pyramidal neurons. In each group, $n = 30$ neurons from 3 brains, 10 per brain. Data from each neuron were collected from 25 serial confocal z-stack images. Data were analyzed using two-tailed unpaired Student's *t*-test with Welch's correction (different variances), $p = 1.69E\text{-}16$. Data represent mean and S.E.M. *$P < 0.05$. See also Supplementary Fig. 4 for more representative images.

this reduction persisted at P45 (Fig. 4*a*–*b*) and P84 (Supplementary Fig. 5c–d), demonstrating that early postnatal loss of CXCL12 led to a fixed deficit in perisomatic inhibitory synapses.

Next, we investigated whether inhibitory synapses were reduced in other target zones on the pyramidal neurons. We stained for pIκBα, which labeled the AIS, and found no differences in the density of GAD65$^+$ punctae on the AIS in *Cxcl12 CKOs* (Fig. 4*c*–*d*). Likewise, there was no change in the density of GAD65$^+$ punctae on *Cxcl12 CKO* distal dendrites in layer I (Fig. 4*e*–*f*). Together, these findings provide evidence that CXCL12 specifically promotes inhibitory synapse formation onto the somata, but not the AIS nor distal dendrites of layer V pyramidal neurons.

CINs that innervate the somata of layer V pyramidal neurons are PV$^+$ basket cells (Huang et al. 2007). Thus, we examined the number and laminar distribution of PV$^+$ CINs in the *Cxcl12 CKO* mPFC. We observed no change in their number and lamination at P16, P28, P45, and P84 (Supplementary Fig. 6a–f), providing evidence that the reduction of inhibitory perisomatic synapses in *Cxcl12 CKOs* was not due to the loss or mislocalization of PV$^+$ CINs, but rather due to a specific defect in their innervation.

CXCL12 Mediates Evoked IPSCs onto Layer V Pyramidal Neurons in the mPFC

To test if the reduction in inhibitory synapses resulted in altered feedforward inhibition onto *Cxcl12 CKO* pyramidal neurons, we compared evoked inhibitory currents in layer V pyramidal neurons within the mPFC of control and *Cxcl12 CKO*. To activate inhibitory interneurons, we transduced mPFC interneurons using an adeno-associated virus (AAV) vector encoding the *Dlx12b* enhancer (Cho et al. 2015) driving channelrhodopsin2 (ChR2-eYFP) expression. We optogenetically-activated these interneurons while simultaneously recording inhibitory currents from layer V pyramidal somata innervated specifically by PV$^+$ basket CINs (Huang et al. 2007), which were voltage-clamped at +10 mV. We delivered 40 Hz light flashes (to preferentially recruit PV$^+$ FSIN outputs) across a high power field to optogenetically-evoke inhibitory currents (Cardin et al. 2009), and assay the ability of layer V microcircuits to generate high frequency inhibition. The amplitudes of optogenetically-evoked IPSCs onto the *Cxcl12 CKO* pyramidal neurons ($n = 32$) were significantly lower than IPSCs onto controls ($n = 31$) throughout a 40 Hz train (Fig. 5*a*).

Layer V pyramidal neurons in the mPFC can be divided into at least two subtypes: thick-tufted, subcortically-projecting type A neurons, with prominent h-current, and thin-tufted, callosally-projecting type B neurons, which lack prominent h-current (Gee et al. 2012). PV$^+$ fast-spiking interneurons (FSINs) preferentially inhibit type A neurons, i.e., optogenetic stimulation of PV$^+$ interneurons elicits more inhibitory current in type A than type B neurons, and the inhibitory connection probability is higher for FSINs-type A pairs than for FSINs-type B pairs (Lee et al. 2014). When we subdivided layer V pyramidal neurons into type A vs. type B neurons (using electrophysiological criteria), we found that optogenetically-evoked IPSCs were selectively compromised in type A neurons of *Cxcl12 CKOs* ($n = 26$) compared to controls ($n = 28$; Fig. 5*b*). By contrast, evoked IPSCs onto type B cells were similar across genotypes (control: $n = 3$; *Cxcl12 CKO*: $n = 6$; Fig. 5*c*). This represents an internal control that suggests the levels of ChR2 expression were not different between controls and *Cxcl12 CKO* mice. Similar to what was previously reported, in control mice we found that the IPSC amplitude in type A neurons was approximately double that in type B neurons (Lee et al. 2014) (Fig. 5*b*–*c*, black bars). Furthermore, we found that while all type A neurons were CXCL12-GFP$^+$, only ~55% of type B neurons had CXCL12-GFP expression in both control and *Cxcl12 CKO* mice at P14-21. These results suggest that CXCL12 specifically promotes inhibition onto type A neurons.

To further explore whether this reduction in IPSCs might reflect decreased connectivity between FSINs and type A neurons, we made paired recordings from individual FSINs (identified by their electrophysiological properties) in current clamp while simultaneously recording from type A neurons in voltage clamp at +10 mV. Consistent with our previous study in which FSINs inhibited nearby type A neurons with a probability ~50% (Lee et al. 2014), we found that the connection probability of FSINs onto type A neurons was 47% (7/15 pairs) in control mice (Fig. 5*d*). We observed a reduced FSIN-type A neuron connection probability of 30% (7/23 pairs) in *Cxcl12 CKO* mice (Fig. 5*d*). Although it did not reach statistical significance, this 36% reduction in connection probability is consistent with the 36% reduction in IPSC amplitude we observed earlier. Finally, we did not observe differences in intrinsic properties for FSINs, type A neurons, or type B neurons, between *Cxcl12 CKO* mice and controls (FSINs, control: n = 17, *Cxcl12 CKO*: $n = 27$, Fig. 5*e*; type A, control: $n = 68$, *Cxcl12 CKO*: $n = 60$, Fig. 5*f*; type B, control: $n = 16$, *Cxcl12 CKO*: $n = 12$, Fig. 5*g*). Thus, the reduction in PV$^+$ inhibitory synapses seems to selectively disrupt inhibition onto type A pyramidal neurons, without affecting connections onto type B neurons, or the intrinsic properties of pyramidal neurons or FSINs.

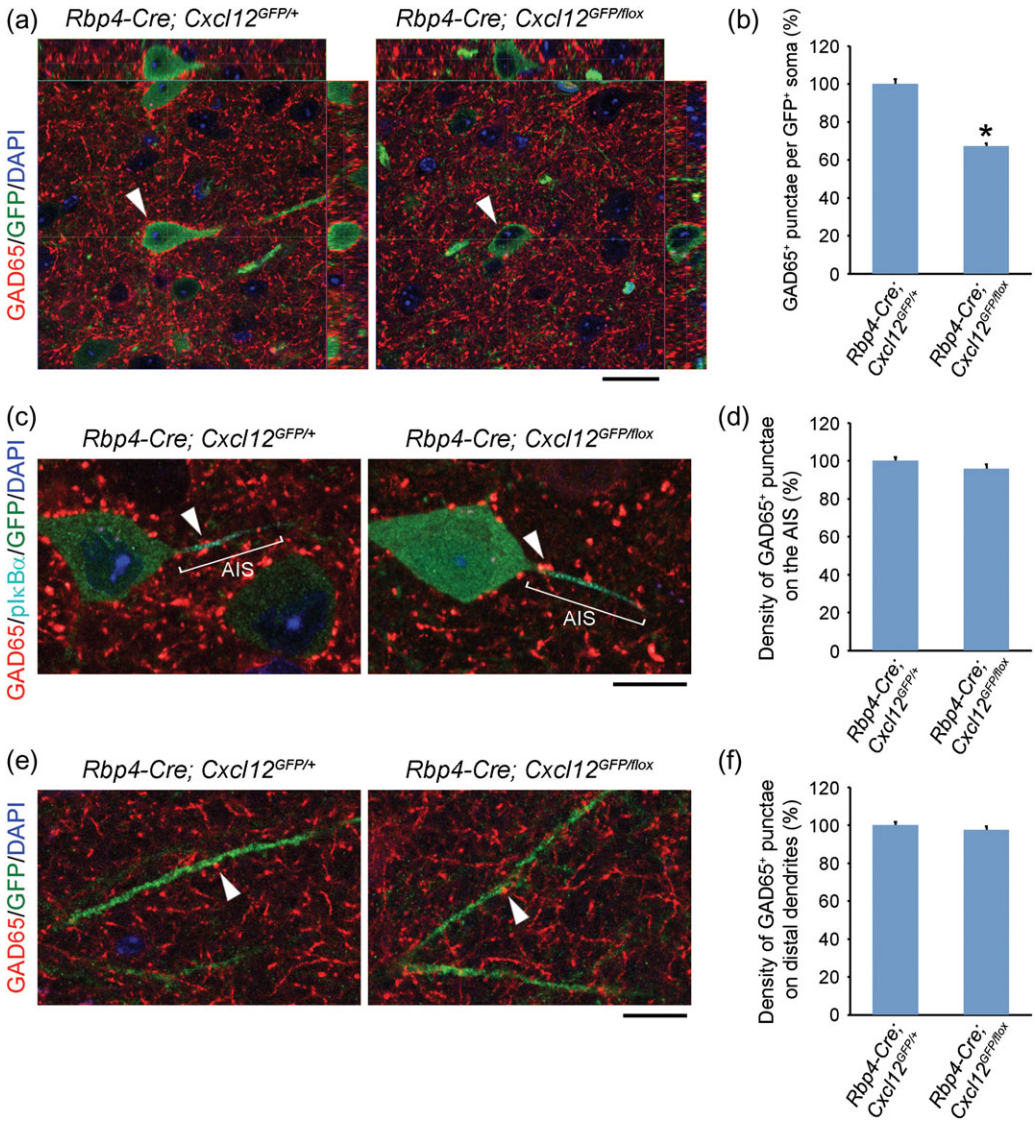

Figure 4. CXCL12 promotes inhibitory perisomatic synapses onto mPFC layer V pyramidal neurons. (*a*) Orthogonal projections from confocal z-stack images (0.5 μm intervals) show decreased perisomatic GAD65$^+$ punctae (red) onto CXCL12-GFP$^+$ pyramidal neurons (indicated by arrowheads) in the P45 *Cxcl12 CKO* mPFC. Scale bar, 20 μm. (*c* and *e*) Confocal images show no change in the density of GAD65$^+$ punctae (red, indicated by arrowheads) on the AIS (*c*) or distal dendrites (*e*) of layer V pyramidal neurons in the P45 *Cxcl12 CKO* mPFC. GFP labeled the whole CXCL12-GFP$^+$ pyramidal neuron, including cell body, the AIS, and distal dendrites. pIκBα (cyan) labeled the AIS. Scale bars, 10 μm. (*b*, *d*, and *f*) Quantification of GAD65$^+$ punctae onto somata (*b*), the AIS (*d*), and distal dendrites (*f*) of CXCL12-GFP$^+$ pyramidal neurons in the P45 mPFC. Data from each soma, AIS, and distal dendrite were collected from 25, 6, and 10 serial confocal z-stack images (0.5 μm intervals), respectively. N = 30 from 3 brains in each group, 10 per brain. Data were analyzed using two-tailed unpaired Student's *t*-test with Welch's correction (different variances, *b*), or without Welch's correction (equal variances, *d* and *f*). P = 5.13E−14 (*b*), 0.1986 (*d*), and 0.3421 (*f*). Data represent mean and S.E.M. *P < 0.05.

Discussion

Here, we report a novel regulatory mode of mPFC activity by CXCL12. We show that in the postnatal mouse mPFC, CXCL12 was predominantly expressed in layer V pyramidal neurons, and highly localized on their cell bodies. Importantly, CXCL12 promoted the specific innervation and synapse formation of CXCR4/7-expressing PV$^+$ interneurons onto the somata, but not distal dendrites or AIS, of layer V pyramidal neurons. Furthermore, CXCL12 enhanced evoked IPSCs onto layer V pyramidal neurons. Thus, reduced CXCL12 expression specifically affected innervation by PV$^+$ basket interneurons (Fig. 6, schema). Given the role of mPFC activity in cognitive function, this study implies that defects in CXCL12-CXCR4/7 signaling could underlie some symptoms of neuropsychiatric disorders.

CXCL12 Regulates Synaptic Transmission and Neuronal Activity through Multiple Mechanisms

In addition to promoting cell migration, several lines of evidence suggest that CXCL12 mediates synaptic transmission and neuronal activity through a variety of mechanisms (Guyon 2014). First, there is in vitro evidence that CXCL12 promotes axon elongation and pathfinding from entorhinal cortical neurons to the dentate gyrus, and thus enhances excitatory synapse formation in the dentate gyrus (Ohshima et al. 2008). This concept is supported by our in vivo finding that CXCL12 promoted axon targeting of PV$^+$ basket CINs. Second, CXCL12 is localized in GABA$^+$ synaptic vesicles, and GABAergic transmission is partially dependent on co-released CXCL12 in the adult dentate gyrus (Bhattacharyya et al. 2008). Furthermore,

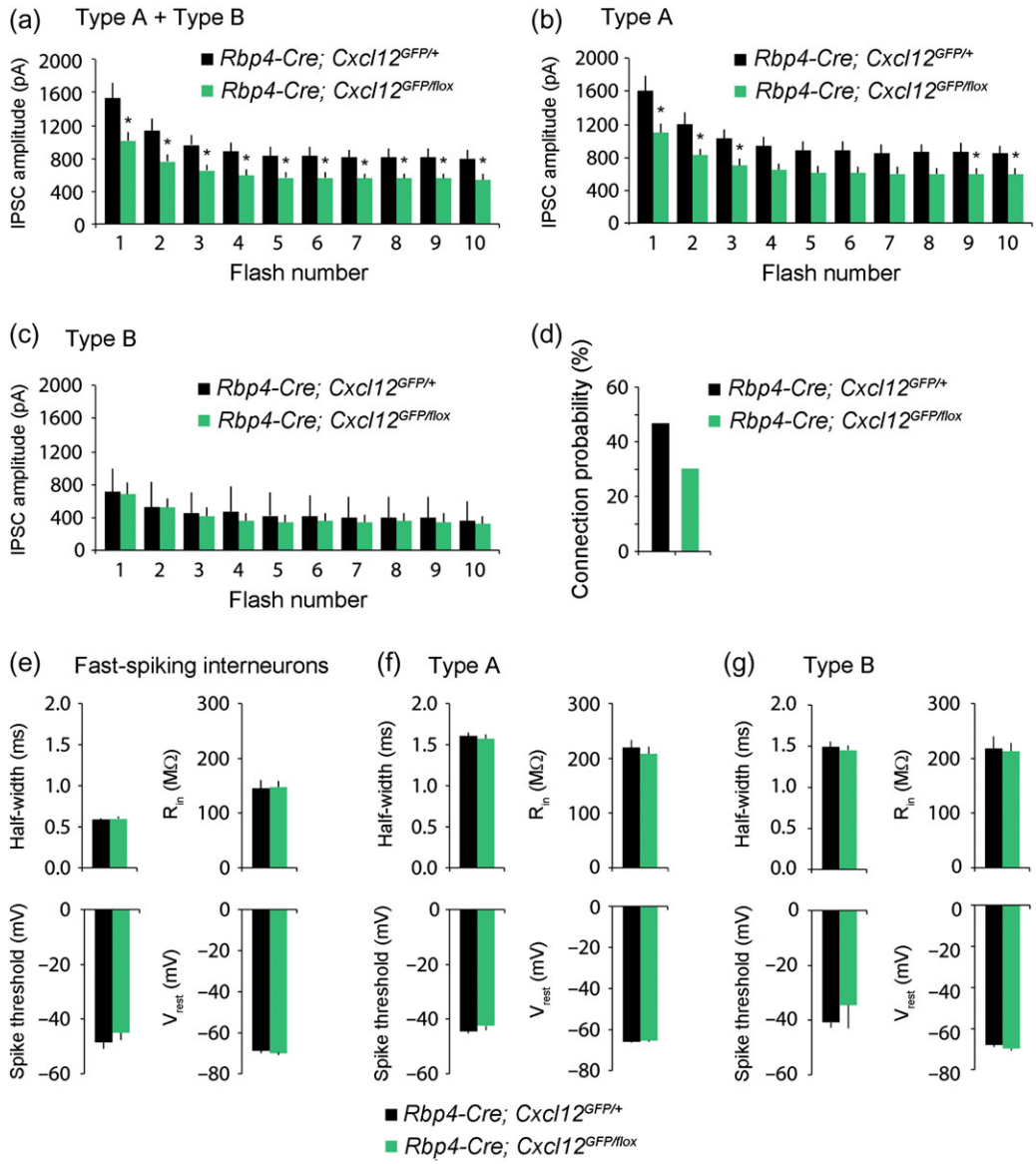

Figure 5. CXCL12 mediates evoked inhibition in type A pyramidal neurons. (*a*) Whole-cell recordings were made from layer V pyramidal neurons in prefrontal brain slices from P42–49 mice, while stimulating ChR2 in *Dlxl12b*-expressing interneurons. Pyramidal neurons were voltage clamped at + 10 mV. The population average of the IPSC amplitudes in pyramidal neurons evoked by 40 Hz optogenetic stimulation of interneurons is lower in *Cxcl12 CKOs* ($n = 32$ from 3 mice) compared to that in controls ($n = 31$ from 3 mice), $p = 0.015$–0.039. (*b*) The population average of the IPSC amplitudes in type A neurons evoked by 40 Hz optogenetic stimulation of interneurons is lower in *Cxcl12 CKOs* ($n = 26$ from 3 mice) compared to that in controls ($n = 28$ from 3 mice), $p = 0.022$–0.0656. (*c*) The population average of the IPSC amplitudes in type B neurons evoked by 40 Hz optogenetic stimulation of interneurons is unchanged in *Cxcl12 CKOs* ($n = 6$ from 2 mice) compared to that in controls ($n = 3$ from 2 mice), $p = 0.655$–0.986. (*d*) There is a decrease in connection probability from FSINs onto type A neurons in *Cxcl12 CKO* (30% = 7/23 pairs from 5 mice) compared to that in controls (47% = 7/15 pairs from 6 mice) at P42–49. (*e–g*) The action potential half-width, input resistance (R_{in}), spike threshold, and resting membrane potential (V_{rest}), calculated from current clamp responses of layer V, P42–49 animals to brief current pulses (–50 pA for input resistance, 100 pA above spiking threshold for other parameters) do not differ in FSINs (control: $n = 17$ from 5 mice, *Cxcl12 CKO*: $n = 27$ from 6 mice, $p = 0.375$–0.930), type A (control: $n = 68$ from 8 mice, *Cxcl12 CKO*: $n = 60$ from 7 mice, $p = 0.432$–0.870), or type B neurons (control: $n = 16$ from 5 mice, *Cxcl12 CKO*: $n = 12$ from 5 mice, $p = 0.215$–0.858). Data were first analyzed with variance tests (*F*-test), and then analyzed using two-tailed unpaired Student's *t*-test with Welch's correction (different variances) or without Welch's correction (equal variances). Data show mean and S.E.M. *$P < 0.05$.

Bhattacharyya et al. reported that CXCL12 treatment increased GABAergic transmission. Similarly, CXCL12 application enhanced inhibitory postsynaptic currents onto serotonin neurons in the rat dorsal raphe nucleus (Heinisch and Kirby 2010), and newly developing neurons induced by transient ischemia (Ardelt et al. 2013). Third, in cultured rat cortical neurons, CXCL12 inhibits NR2B expression, a subunit of *N*-methyl-D-aspartic acid (NMDA) receptors, through activating histone deacetylases (HDACs), and thus decreases NMDA-induced calcium responses (Nicolai et al. 2010). Fourth, in rat hippocampal neurons, CXCL12 activates the voltage-gated potassium channel Kv2.1 through altering its phosphorylation and plasma membrane localization, thereby enhancing Kv2.1 currents (Shepherd et al. 2012). Lastly, like CXCR4 and CXCR7, the $GABA_B$ receptors, $GABA_B1$ and $GABA_B2$, are G-protein-coupled receptors (GPCRs). It is hypothesized that these receptors may regulate synaptic currents by directly interacting through heterodimerization, or indirectly through activating common signaling pathways

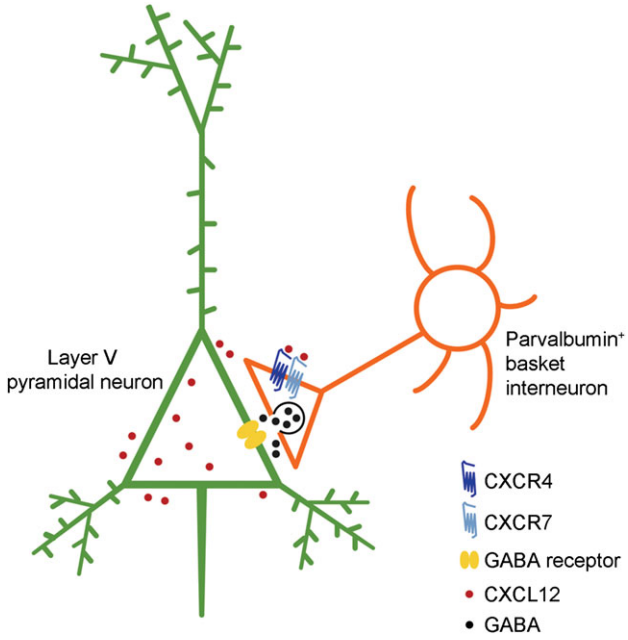

Figure 6. Model of CXCL12 function(s) in the mPFC. In the postnatal mPFC, CXCL12 is detected around the extracellular surface of layer V pyramidal neurons (shown in green), while its receptors CXCR4 and CXCR7 are present at the axon terminals of PV^+ basket interneurons (shown in orange). CXCL12 promotes targeting of PV^+ basket interneuron axons, the number of inhibitory perisomatic synapses, and IPSCs onto layer V pyramidal neurons.

(Guyon 2014). In sum, CXCL12 may mediate synaptic activity through multiple mechanisms, including regulating synapse numbers, transcription, and post-translational modification of synaptic components.

Evidence that CXCL12 Regulates CIN Lamination

CXCL12 is well characterized as a chemoattractant for cell migration (Sanchez-Martin et al. 2013), including tangential migration of immature CINs (Stumm et al. 2003; Tiveron et al. 2006; Sanchez-Alcaniz et al. 2011; Wang et al. 2011). We postulated that CXCL12 may regulate CIN radial migration for several reasons, including its neonatal expression in layer V pyramidal neurons (Vogt et al. 2014) (Supplementary Fig. 1b). Although we did not observe a CIN lamination defect in *Cxcl12 CKOs* (Supplementary Fig. 1c–e), we did find abnormal CIN lamination using the MGE transplantation assay (Supplementary Fig. 1f–g). These discrepant results may be due to a few reasons. First, the transplanted cells were from E14.5 MGE cells and their response to the cortical environment of *Cxcl12 CKOs* might be different than the endogenous P2 CINs. Secondly, *Rbp4-Cre* may be expressed too late to remove sufficient *Cxcl12*. Indeed, at P1 only 56% of CXCL12-GFP^+ cells co-expressed Rbp4-Cre (Supplementary Fig. 1b), a stage when CINs have already migrated into the cortex (Bartolini et al. 2013). Consequently, a layer V-specific Cre that is expressed earlier may answer whether CXCL12 regulates CIN radial migration.

Altered CXCL12-CXCR4/7 Signaling Might Contribute to Neuropsychiatric Disorders

Higher levels of cognitive control require gamma (30–80 Hz) oscillations, which is dependent on PV^+ basket CIN inhibitory inputs onto pyramidal neurons. As a result, dysfunction of PV^+ CINs is likely to be deleterious for cognition (Lewis et al. 2012). Consistently, defects in PFC PV^+ interneuron may be a risk factor for schizophrenia (Volk and Lewis 2014). CXCL12-CXCR4/7 signaling defects, based on abnormal *Cxcr4/7* expression in the PFC, are postulated to contribute to CIN dysfunction in schizophrenia (Volk et al. 2015). Moreover, *Cxcl12* expression is decreased in the olfactory neuronal layers of schizophrenia patients (Toritsuka et al. 2013). CXCL12-CXCR4 signaling is implicated in CIN migration deficits in the mouse models of 22q11 deletion syndrome (22q11DS), a chromosome disorder frequently associated with bipolar disorder and schizophrenia (Meechan et al. 2012; Toritsuka et al. 2013). Furthermore, CXCR4 depletion in PV^+ CINs increases motor stereotypy, a behavior found in autism and schizophrenia (Cash-Padgett et al. 2016). These studies, taken together with our finding that CXCL12 promotes IPSCs onto layer V pyramidal neurons in the mPFC, provide substantial evidence that CXCL12-CXCR4/7 signaling regulates mPFC function, and disruption of this signaling may contribute to neuropsychiatric disorders.

Author Contributions

P.-R.W., K.K.A.C., D.V., V.S.S., and J.L.R.R. designed experiments. P.-R.W. and D.V. performed MGE transplantation. K.K.A.C. performed the electrophysiological assays. All the rest of the experiments were conducted by P.-R.W. P.-R.W. and K.K.A.C. analyzed the data. P.-R.W., K.K.A.C., D.V., V.S.S., and J.L.R.R. wrote the manuscript.

Supplementary Material

Supplementary material can be found at: http://www.cercor.oxfordjournals.org.

Funding

National Institutes of Health (NIMH R37 MH049428 to J.L.R.R. and 1R01MH106507-01 to V.S.S.), Brain and Behavior Foundation (NARSAD Young Investigator Award to K.K.A.C.), and National Science Council of Taiwan (NSC 102-2917-I-564-007 to P.-R.W.).

Notes

The mouse strain used for this research project, STOCK Tg (Rbp4-cre)KL100Gsat/Mmucd, identification number 031125-UCD, was obtained from the Mutant Mouse Regional Resource Center, a NIH funded strain repository, and was donated to the MMRRC by the NINDS funded GENSAT BAC transgenic project. *Conflict of Interest:* J.L.R.R. is a founder and on the SAB of Neurona.

References

Abe P, Molnar Z, Tzeng YS, Lai DM, Arnold SJ, Stumm R. 2015. Intermediate progenitors facilitate intracortical progression of thalamocortical axons and interneurons through CXCL12 chemokine signaling. J Neurosci. 35:13053–13063.

Ara T, Tokoyoda K, Sugiyama T, Egawa T, Kawabata K, Nagasawa T. 2003. Long-term hematopoietic stem cells require stromal cell-derived factor-1 for colonizing bone marrow during ontogeny. Immunity. 19:257–267.

Ardelt AA, Bhattacharyya BJ, Belmadani A, Ren D, Miller RJ. 2013. Stromal derived growth factor-1 (CXCL12) modulates

synaptic transmission to immature neurons during post-ischemic cerebral repair. Exp Neurol. 248:246–253.

Bartolini G, Ciceri G, Marin O. 2013. Integration of GABAergic interneurons into cortical cell assemblies: lessons from embryos and adults. Neuron. 79:849–864.

Bhattacharyya BJ, Banisadr G, Jung H, Ren D, Cronshaw DG, Zou Y, Miller RJ. 2008. The chemokine stromal cell-derived factor-1 regulates GABAergic inputs to neural progenitors in the postnatal dentate gyrus. J Neurosci. 28:6720–6730.

Cardin JA, Carlen M, Meletis K, Knoblich U, Zhang F, Deisseroth K, Tsai LH, Moore CI. 2009. Driving fast-spiking cells induces gamma rhythm and controls sensory responses. Nature. 459:663–667.

Cash-Padgett T, Sawa A, Jaaro-Peled H. 2016. Increased stereotypy in conditional Cxcr4 knockout mice. Neurosci Res. 105:75–9.

Cho KK, Sohal VS. 2014. Optogenetic approaches for investigating neural pathways implicated in schizophrenia and related disorders. Hum Mol Genet. 23:R64–68.

Cho KK, Hoch R, Lee AT, Patel T, Rubenstein JL, Sohal VS. 2015. Gamma rhythms link prefrontal interneuron dysfunction with cognitive inflexibility in Dlx5/6(+/–) mice. Neuron. 85:1332–1343.

Fazzari P, Paternain AV, Valiente M, Pla R, Lujan R, Lloyd K, Lerma J, Marin O, Rico B. 2010. Control of cortical GABA circuitry development by Nrg1 and ErbB4 signalling. Nature. 464:1376–1380.

Gee S, Ellwood I, Patel T, Luongo F, Deisseroth K, Sohal VS. 2012. Synaptic activity unmasks dopamine D2 receptor modulation of a specific class of layer V pyramidal neurons in prefrontal cortex. J Neurosci. 32:4959–4971.

Greenbaum A, Hsu YM, Day RB, Schuettpelz LG, Christopher MJ, Borgerding JN, Nagasawa T, Link DC. 2013. CXCL12 in early mesenchymal progenitors is required for haematopoietic stem-cell maintenance. Nature. 495:227–230.

Guyon A. 2014. CXCL12 chemokine and GABA neurotransmitter systems crosstalk and their putative roles. Front Cell Neurosci. 5:115.

Heinisch S, Kirby LG. 2010. SDF-1alpha/CXCL12 enhances GABA and glutamate synaptic activity at serotonin neurons in the rat dorsal raphe nucleus. Neuropharmacology. 58:501–514.

Huang ZJ, Di Cristo G, Ango F. 2007. Development of GABA innervation in the cerebral and cerebellar cortices. Nat Rev Neurosci. 8:673–686.

Kessaris N, Magno L, Rubin AN, Oliveira MG. 2014. Genetic programs controlling cortical interneuron fate. Curr Opin Neurobiol. 26:79–87.

Lee AT, Gee SM, Vogt D, Patel T, Rubenstein JL, Sohal VS. 2014. Pyramidal neurons in prefrontal cortex receive subtype-specific forms of excitation and inhibition. Neuron. 81:61–68.

Lewis DA, Curley AA, Glausier JR, Volk DW. 2012. Cortical parvalbumin interneurons and cognitive dysfunction in schizophrenia. Trends Neurosci. 35:57–67.

Li G, Adesnik H, Li J, Long J, Nicoll RA, Rubenstein JL, Pleasure SJ. 2008. Regional distribution of cortical interneurons and development of inhibitory tone are regulated by Cxcl12/Cxcr4 signaling. J Neurosci. 28:1085–1098.

Madisen L, Zwingman TA, Sunkin SM, Oh SW, Zariwala HA, Gu H, Ng LL, Palmiter RD, Hawrylycz MJ, Jones AR, et al. 2010. A robust and high-throughput Cre reporting and characterization system for the whole mouse brain. Nat Neurosci. 13:133–140.

Marin O. 2013. Cellular and molecular mechanisms controlling the migration of neocortical interneurons. Eur J Neurosci. 38:2019–2029.

Meechan DW, Tucker ES, Maynard TM, LaMantia AS. 2012. Cxcr4 regulation of interneuron migration is disrupted in 22q11.2 deletion syndrome. Proc Natl Acad Sci USA. 109:18601–18606.

Nagasawa T, Hirota S, Tachibana K, Takakura N, Nishikawa S, Kitamura Y, Yoshida N, Kikutani H, Kishimoto T. 1996. Defects of B-cell lymphopoiesis and bone-marrow myelopoiesis in mice lacking the CXC chemokine PBSF/SDF-1. Nature. 382:635–638.

Nicolai J, Burbassi S, Rubin J, Meucci O. 2010. CXCL12 inhibits expression of the NMDA receptor's NR2B subunit through a histone deacetylase-dependent pathway contributing to neuronal survival. Cell Death Dis. 1:e33.

Ohshima Y, Kubo T, Koyama R, Ueno M, Nakagawa M, Yamashita T. 2008. Regulation of axonal elongation and pathfinding from the entorhinal cortex to the dentate gyrus in the hippocampus by the chemokine stromal cell-derived factor 1 alpha. J Neurosci. 28:8344–8353.

Potter GB, Petryniak MA, Shevchenko E, McKinsey GL, Ekker M, Rubenstein JL. 2009. Generation of Cre-transgenic mice using Dlx1/Dlx2 enhancers and their characterization in GABAergic interneurons. Mol Cell Neurosci. 40:167–186.

Sanchez-Alcaniz JA, Haege S, Mueller W, Pla R, Mackay F, Schulz S, Lopez-Bendito G, Stumm R, Marin O. 2011. Cxcr7 controls neuronal migration by regulating chemokine responsiveness. Neuron. 69:77–90.

Sanchez-Martin L, Sanchez-Mateos P, Cabanas C. 2013. CXCR7 impact on CXCL12 biology and disease. Trends Mol Med. 19:12–22.

Shepherd AJ, Loo L, Gupte RP, Mickle AD, Mohapatra DP. 2012. Distinct modifications in Kv2.1 channel via chemokine receptor CXCR4 regulate neuronal survival-death dynamics. J Neurosci. 32:17725–17739.

Sohal VS, Huguenard JR. 2005. Inhibitory coupling specifically generates emergent gamma oscillations in diverse cell types. Proc Natl Acad Sci USA. 102:18638–18643.

Sohal VS, Zhang F, Yizhar O, Deisseroth K. 2009. Parvalbumin neurons and gamma rhythms enhance cortical circuit performance. Nature. 459:698–702.

Stumm RK, Zhou C, Ara T, Lazarini F, Dubois-Dalcq M, Nagasawa T, Hollt V, Schulz S. 2003. CXCR4 regulates interneuron migration in the developing neocortex. J Neurosci. 23:5123–5130.

Tiveron MC, Rossel M, Moepps B, Zhang YL, Seidenfaden R, Favor J, Konig N, Cremer H. 2006. Molecular interaction between projection neuron precursors and invading interneurons via stromal-derived factor 1 (CXCL12)/CXCR4 signaling in the cortical subventricular zone/intermediate zone. J Neurosci. 26:13273–13278.

Tiveron MC, Boutin C, Daou P, Moepps B, Cremer H. 2010. Expression and function of CXCR7 in the mouse forebrain. J Neuroimmunol. 224:72–79.

Toritsuka M, Kimoto S, Muraki K, Landek-Salgado MA, Yoshida A, Yamamoto N, Horiuchi Y, Hiyama H, Tajinda K, Keni N, et al. 2013. Deficits in microRNA-mediated Cxcr4/Cxcl12 signaling in neurodevelopmental deficits in a 22q11 deletion syndrome mouse model. Proc Natl Acad Sci USA. 110:17552–17557.

Uhlhaas PJ, Singer W. 2010. Abnormal neural oscillations and synchrony in schizophrenia. Nat Rev Neurosci. 11:100–113.

Vogt D, Hunt RF, Mandal S, Sandberg M, Silberberg SN, Nagasawa T, Yang Z, Baraban SC, Rubenstein JL. 2014. Lhx6

directly regulates Arx and CXCR7 to determine cortical interneuron fate and laminar position. Neuron. 82:350–364.

Vogt D, Wu PR, Sorrells SF, Arnold C, Alvarez-Buylla A, Rubenstein JL. 2015. Viral-mediated labeling and transplantation of medial ganglionic eminence (MGE) cells for in vivo studies. J Vis Exp. 98:e52740.

Volk DW, Lewis DA. 2014. Early developmental disturbances of cortical inhibitory neurons: contribution to cognitive deficits in schizophrenia. Schizophr Bull. 40:952–957.

Volk DW, Chitrapu A, Edelson JR, Lewis DA. 2015. Chemokine receptors and cortical interneuron dysfunction in schizophrenia. Schizophr Res. 167:12–17.

Wang Y, Li G, Stanco A, Long JE, Crawford D, Potter GB, Pleasure SJ, Behrens T, Rubenstein JL. 2011. CXCR4 and CXCR7 have distinct functions in regulating interneuron migration. Neuron. 69:61–76.

Xu Q, Tam M, Anderson SA. 2008. Fate mapping Nkx2.1-lineage cells in the mouse telencephalon. J Comp Neurol. 506:16–29.